Improvement of Visible-Light H_2 Evolution Activity of $Pb_2Ti_2O_{5.4}F_{1.2}$ Photocatalyst by Coloading of Rh and Pd Cocatalysts

Kenta Aihara,[a] Kosaku Kato,[b] Tomoki Uchiyama,[c] Shuhei Yasuda,[d] Toshiyuki Yokoi,[d] Akira Yamakata,[b] Yoshiharu Uchimoto,[c] and Kazuhiko Maeda*[a]

Abstract: $Pb_2Ti_2O_{5.4}F_{1.2}$ modified with various metal cocatalysts was studied as a photocatalyst for visible-light H_2 evolution. Although unmodified $Pb_2Ti_2O_{5.4}F_{1.2}$ showed negligible activity, modification of its surface with Rh led to the best observed promotional effect among the $Pb_2Ti_2O_{5.4}F_{1.2}$ samples modified with a single metal cocatalyst. The H_2 evolution activity was further enhanced by coloading with Pd; the Rh–Pd/$Pb_2Ti_2O_{5.4}F_{1.2}$ photocatalyst showed 3.2 times greater activity than the previously reported Pt/$Pb_2Ti_2O_{5.4}F_{1.2}$. X-ray absorption fine-structure spectroscopy, photoelectrochemical, and transient absorption spectroscopy measurements indicated that the coloaded Rh and Pd species, which were partially alloyed on the $Pb_2Ti_2O_{5.4}F_{1.2}$ surface, improved the electron-capturing ability, thereby explaining the high activity of the coloaded Rh–Pd/$Pb_2Ti_2O_{5.4}F_{1.2}$ catalyst toward H_2 evolution.

Introduction

To develop photocatalysts that can absorb visible light, researchers have actively studied mixed-anion compounds with a controllable bandgap in recent years.[1–3] $Pb_2Ti_2O_{5.4}F_{1.2}$ is a visible-light-responsive mixed-anion photocatalyst with a bandgap of 2.4 eV.[4,5] The valence-band maximum (VBM) of $Pb_2Ti_2O_{5.4}F_{1.2}$ consists of O $2p$ orbitals, whereas that of ordinary mixed-anion compounds such as oxynitrides and oxysulfides is composed of N $2p$ and S $3p$ orbitals, respectively. Therefore, $Pb_2Ti_2O_{5.4}F_{1.2}$ is expected to function as a highly stable photocatalyst that does not undergo self-oxidation by valence-band holes. However, the activity of the $Pb_2Ti_2O_{5.4}F_{1.2}$ photocatalyst is unsatisfactory.

Toward efficient H_2 evolution, cocatalysts, typically in the form of nanoparticles of metals (or metal oxides), are known to strongly affect the photocatalytic activity.[6–11] A cocatalyst on a semiconductor photocatalyst has two main functions: (1) capturing excited electrons and/or holes and (2) hosting active reaction sites (Scheme 1).[12,13] In general, nanoparticulate Pt is a good cocatalyst for H_2 evolution for many semiconductor photocatalysts because of its excellent catalytic function of proton reduction, as already well documented in the electrochemistry field. However, Pt is not always the best-performing cocatalyst for a photocatalyst, likely because of the complicated charge-transfer process at the Pt/photocatalyst interface.[6,14]

Therefore, investigating cocatalysts is important for improving the photocatalytic activity of semiconductor photocatalysts,

[a] K. Aihara, Prof. K. Maeda
Department of Chemistry, School of Science
Tokyo Institute of Technology
2-12-1-NE-2 Ookayama, Meguro-ku, Tokyo 152-8550 (Japan)
E-mail: maedak@chem.titech.ac.jp

[b] Dr. K. Kato, Prof. A. Yamakata
Graduate School of Engineering
Toyota Technological Institute
2-12-1 Hisakata, Tempaku, Nagoya 468-8511 (Japan)
and
Present address: Graduate School of Natural Science and Technology,
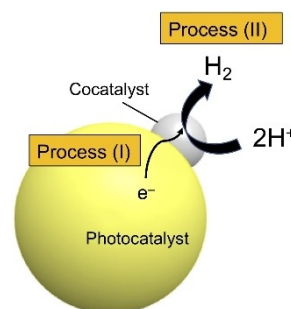Okayama University, 3-1-1 Tsushima-naka, Kita-ku, Okayama (Japan)

[c] Dr. T. Uchiyama, Prof. Y. Uchimoto
Graduate School of Human and Environmental Studies
Kyoto University
Yoshidanihonmatsu-cho, Sakyo-ku, Kyoto 606-8501 (Japan)

[d] Dr. S. Yasuda, Prof. T. Yokoi
Nanospace Catalysis Unit, Institute of Innovative Research
Tokyo Institute of Technology
Yokohama 226-8503 (Japan)

Scheme 1. Schematic of electron transfer from a photocatalyst to a loaded cocatalyst (Process I); H_2 evolution (Process II) is also shown.

especially those that are newly developed. Thus far, numerous photocatalysts, including metal oxides, sulfides, oxynitrides, and organic polymers, have been investigated. However, to the best of our knowledge, the literature contains no report on the photocatalytic properties of an oxyfluoride for H_2 evolution with respect to cocatalyst loading. Thus, knowledge of the photocatalytic properties of oxyfluorides remains inadequate.

In the present study, optimal cocatalysts for the $Pb_2Ti_2O_{5.4}F_{1.2}$ photocatalyst were investigated to improve its H_2 production activity. In addition, how the optimal cocatalyst works is discussed on the basis of the results of photoelectrochemical and transient absorption spectroscopy measurements.

Results and Discussion

Photocatalytic activities of metal-loaded $Pb_2Ti_2O_{5.4}F_{1.2}$

Various metals (e.g., Ru, Rh, Pd, Ir, Pt, and Au) were investigated as cocatalysts for the $Pb_2Ti_2O_{5.4}F_{1.2}$ photocatalyst using a batch-type reactor under 365 nm LED light (see Figure S1a for the spectral irradiance) to identify the optimal metal cocatalyst.
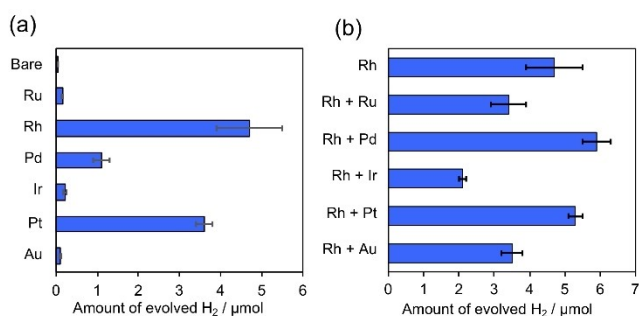

Figure 1. Photocatalytic H_2 evolution activities of $Pb_2Ti_2O_{5.4}F_{1.2}$ loaded with (a) various metal cocatalysts (0.5 wt%) and (b) Rh and various metals (0.5 wt% each). Reaction conditions: catalyst, 4 mg (0.5 wt% cocatalyst photo-deposited in situ); reaction solution, MeCN:TEOA:H_2O mixture (89:10:1 v/v/v) 4 mL; light source, LED lamp (365 nm); reaction time, 20 h.
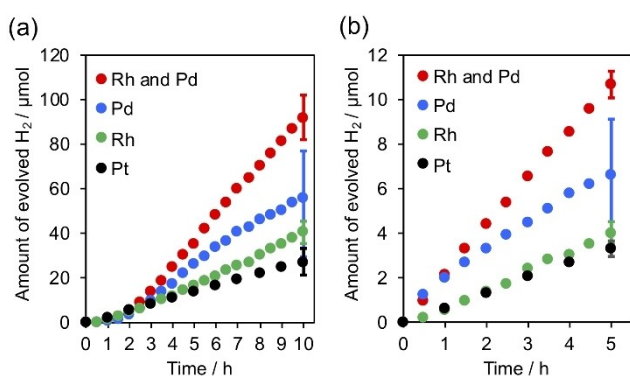

Figure 2. Time courses of H_2 evolution by modified $Pb_2Ti_2O_{5.4}F_{1.2}$ photocatalysts under irradiation with (a) UV ($\lambda > 350$ nm) and (b) visible light ($\lambda > 400$ nm). Reaction conditions: catalyst, 100 mg (0.5 wt% cocatalyst photo-deposited in situ); reaction solution, MeCN:TEOA mixture (130:10 v/v) containing 1 mL water, 140 mL; light source, 300 W Xe lamp.

These metals are known to function as cocatalysts for photocatalytic H_2 evolution.[9,15] Whereas unmodified $Pb_2Ti_2O_{5.4}F_{1.2}$ exhibited little activity, $Pb_2Ti_2O_{5.4}F_{1.2}$ modified with the metals via an in situ photodeposition method demonstrated enhanced activity (Figure 1a). Among the metals examined, Rh resulted in the highest H_2 generation activity when loaded as a cocatalyst onto $Pb_2Ti_2O_{5.4}F_{1.2}$.

The H_2 generation activity was found to be further increased by the coloading of Rh and Pd (Figure 1b). The activity of Rh/Pd-coloaded $Pb_2Ti_2O_{5.4}F_{1.2}$ was ~30% higher than that of the Rh-loaded analogue. Coloading of Rh and Pt could moderately improve the H_2 evolution activity but was not as effective as the coloading of Rh and Pd.

Figure 2 shows the time courses of H_2 evolution by the Rh/Pd-coloaded $Pb_2Ti_2O_{5.4}F_{1.2}$, along with that of the previously reported Pt-loaded analogue.[16] These experiments were conducted using a closed gas circulation system with a 300 W Xe lamp, which could provide more photons in visible light region (Figure S1b). Under this condition, the Pd/$Pb_2Ti_2O_{5.4}F_{1.2}$ showed a relatively high initial H_2 evolution rate; however, the H_2 evolution rate degraded over time, with a large experimental error. By contrast, the coloaded photocatalyst produced H_2 stably and was ~3.2 times more active than the previously reported Pt-loaded photocatalyst both under UV irradiation and under visible-light irradiation. The enhancement factor of 3.2 achieved by the coloaded Rh and Pd under high-intensity light irradiation (Figure 2b) was greater than that obtained under LED irradiation (Figure 1b). This difference suggests that the activity improvement by coloading is more pronounced under irradiation with high-intensity light.

Characterization of the loaded Rh and Pd species

We attempted to examine how Rh and Pd were deposited onto the $Pb_2Ti_2O_{5.4}F_{1.2}$. However, obtaining a clear picture was difficult. As shown in Figure 3, scanning electron microscopy (SEM) observations revealed that the surface of the unmodified $Pb_2Ti_2O_{5.4}F_{1.2}$ was rough, containing numerous irregularly shaped smaller particles. The Rh–Pd/$Pb_2Ti_2O_{5.4}F_{1.2}$ exhibited a similar morphological character, which made it difficult to
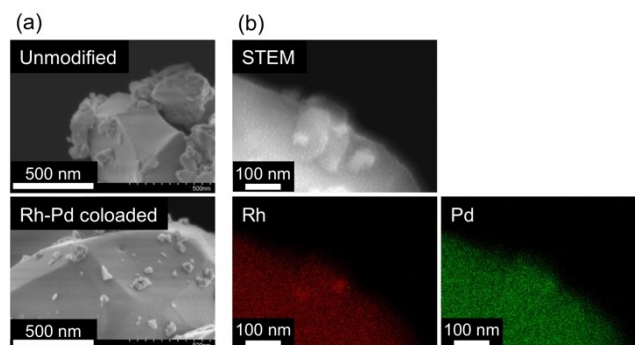

Figure 3. a) SEM and b) STEM/EDS mapping images of the Rh–Pd/$Pb_2Ti_2O_{5.4}F_{1.2}$.

Chemistry–A European Journal

Research Article
doi.org/10.1002/chem.202200875

Chemistry
Europe
European Chemical
Societies Publishing

distinguish any photodeposited species from the smaller $Pb_2Ti_2O_{5.4}F_{1.2}$ particles. We conducted energy-dispersive X-ray spectroscopy (EDS) measurements with care to avoid beam-damage to the sample. In some cases, Rh and Pd signals were observed close to each other (Figure 3b); however, we could not determine whether the same was true for other locations. Observations by transmission electron microscopy (TEM) also failed, as the electron densities of Rh and Pd are very similar and the sample could not withstand the strong electron beams during the TEM observations.

To examine the electronic state, the valence state of Rh and Pd species photodeposited onto $Pb_2Ti_2O_{5.4}F_{1.2}$ were characterized by XAFS measurement. The Rh–K edge X-ray absorption near-edge structure (XANES) spectra for $Rh/Pb_2Ti_2O_{5.4}F_{1.2}$, $Rh–Pd/Pb_2Ti_2O_{5.4}F_{1.2}$, and some reference materials are shown in Figure 4a. The Rh–K edge XANES spectrum for $Rh–Pd/Pb_2Ti_2O_{5.4}F_{1.2}$ is similar to that for $Rh/Pb_2Ti_2O_{5.4}F_{1.2}$. By comparing the spectra of the samples with those of the reference materials, we found that the loaded Rh species in the two samples was a mixture of oxide and metal. The Rh–K edge XANES spectrum for the $Rh–Pd/Pb_2Ti_2O_{5.4}F_{1.2}$ could be reproduced by a linear combination of the spectra of the Rh foil and Rh_2O_3 references, and the $Rh:Rh_2O_3$ ratio for the $Rh–Pd/Pb_2Ti_2O_{5.4}F_{1.2}$ sample was found to be 56:44. However, the $Rh:Rh_2O_3$ ratio for the $Rh/Pb_2Ti_2O_{5.4}F_{1.2}$ was 52:48. Therefore, the $Rh–Pd/Pb_2Ti_2O_{5.4}F_{1.2}$

sample contained a higher density of metallic Rh than the $Rh/Pb_2Ti_2O_{5.4}F_{1.2}$ sample.

Fourier transforms (FTs) of the k^2-weighted Rh–K edge EXAFS data confirmed the existence of Rh–O and metallic Rh–M ($M =$ Rh or Pd) bonds at $R \approx 1.5$ and 2.4 Å, respectively. However, no peak derived from Rh-(O)-Rh bonding (e.g., at ~ 3 Å) was observed, suggesting the absence of bulk Rh_2O_3 species. The absence of the Rh–Cl peak for $Na_3RhCl_6 \cdot nH_2O$ also indicates complete decomposition of the precursor during the photodeposition process.

As shown in Figure 4c, the peaks in the Pd–K edge XANES spectra for the two samples were located at slightly lower energies than those for the Pd foil reference, indicating that the Pd species are more electron-rich than Pd foil. This result might be attributable to an electron-donation effect of the $Pb_2Ti_2O_{5.4}F_{1.2}$ support, which is an n-type semiconductor.[4,17]

Although no difference was observed in the Pd–K edge XANES spectra between singly loaded and coloaded samples, the FT-EXAFS spectra indicated somewhat different bonding natures in these samples (Figure 4d). The Pd foil gave a strong peak at ~ 2.7 Å, which is attributed to Pd–Pd bonds. However, the peaks due to Pd-M bonds ($M =$ Pd or Rh) in the spectra of the $Pd/Pb_2Ti_2O_{5.4}F_{1.2}$ and $Rh–Pd/Pb_2Ti_2O_{5.4}F_{1.2}$ samples were located at longer distances than the Pd–Pd peak position in the spectrum of the Pd foil reference. This result indicates that the bond length for Pd-M in the two samples was larger than that for Pd–Pd in the Pd foil. This finding is consistent with the results of the Pd–K edge XANES measurements (Figure 4c), which indicated that the Pd species in the two samples was in an electron-rich state. The Pd-M bond length in the $Rh–Pd/Pb_2Ti_2O_{5.4}F_{1.2}$ was smaller than that in the $Pd/Pb_2Ti_2O_{5.4}F_{1.2}$, strongly suggesting that partial alloying occurred between Rh and Pd in the $Rh–Pd/Pb_2Ti_2O_{5.4}F_{1.2}$ given that the lattice constants of Rh and Pd are $a = 3.71559$ and 3.8898 Å, respectively. Rh and Pd have been reported to form an alloy over the full composition range.[18–20] However, the formation of a core/shell-like structure (i.e., Rh on Pd or Pd on Rh) is unlikely given the surface atomic ratios of Rh/Ti and Pd/Ti, which were almost constant between singly and doubly loaded samples (Table S1).

The valence states of Rh and Pd species were also investigated by X-ray photoelectron spectroscopy (XPS). The XPS measurements lead to the same conclusions as the XAFS measurements (Figure S2). Although the relative locations of the Rh and Pd species in the $Rh–Pd/Pb_2Ti_2O_{5.4}F_{1.2}$ could not be identified by electron microscopy, XAFS measurements gave clearer information about their "locations" based on their electronic states.

Factors affecting the photocatalytic activity

To investigate whether the reduction or oxidation reaction was promoted by the coloading of Rh and Pd, we conducted photoelectrochemical measurements using modified $Pb_2Ti_2O_{5.4}F_{1.2}$ electrodes under visible light. Because an n-type semiconductor shows a rectifying action, its photooxidation

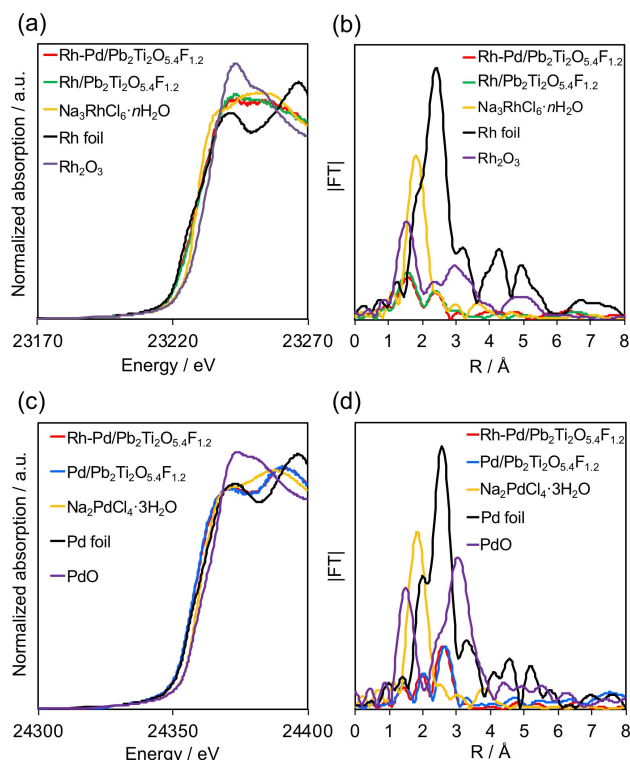**Figure 4.** Results of XAFS measurement for modified $Pb_2Ti_2O_{5.4}F_{1.2}$. Rh–K edge (a) XANES and (b) FT-EXAFS spectra. Pd–K edge (c) XANES and (d) FT-EXAFS spectra. Note that FT-EXAFS cannot distinguish Pd–Rh, Pd–Pd, and Rh–Rh bonds because Pd and Rh have similar atomic numbers (i.e., approximately the same backscattering amplitude).

Chemistry–A European Journal

Research Article
doi.org/10.1002/chem.202200875

**Chemistry
Europe**
European Chemical
Societies Publishing

ability can be monitored using photocurrent measurements.[21,22]

Figure 5 shows current-voltage curves for modified $Pb_2Ti_2O_{5.4}F_{1.2}$ electrodes under intermittent irradiation with visible light ($\lambda > 400$ nm) in the presence of triethanolamine (TEOA) as an electron donor. These results show that the photocurrent density for TEOA oxidation decreased in the order $Pb_2Ti_2O_{5.4}F_{1.2}$, $Rh/Pb_2Ti_2O_{5.4}F_{1.2}$, $Pd/Pb_2Ti_2O_{5.4}F_{1.2}$, and $Rh–Pd/Pb_2Ti_2O_{5.4}F_{1.2}$. Thus, the loading of Rh or Pd as well as their coloading lowered the efficiency of photooxidation reactions on the $Pb_2Ti_2O_{5.4}F_{1.2}$ surface, most likely because the loaded metal species reduced the available area for oxidation reactions. Nevertheless, the photoreduction activity of the $Pb_2Ti_2O_{5.4}F_{1.2}$ during H_2 evolution was improved by Rh and Pd loading (Figure 2). This result suggests that the promotional effect of Rh and Pd coloading on the $Pb_2Ti_2O_{5.4}F_{1.2}$ resulted from improvements of the photoreduction processes.

To further investigate the behavior of photogenerated electrons in the modified $Pb_2Ti_2O_{5.4}F_{1.2}$, we carried out transient absorption measurements. Figure 6 shows the decay kinetics of the transient absorption signals recorded at 2000 cm^{-1}, which are attributed to photogenerated free electrons and/or shallowly trapped electrons in the $Pb_2Ti_2O_{5.4}F_{1.2}$.[23,24] A smaller Δabsorbance and its f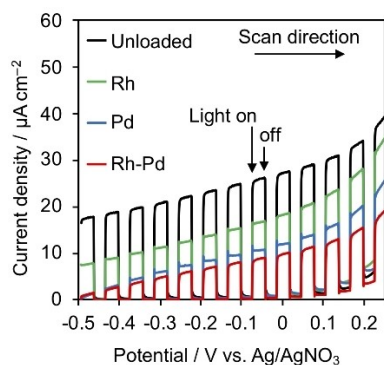aster decay indicate more efficient trapping of photogenerated electrons.[23,24] The $Rh/Pb_2Ti_2O_{5.4}F_{1.2}$ showed a smaller Δabsorbance than $Pd/Pb_2Ti_2O_{5.4}F_{1.2}$ and bare $Pb_2Ti_2O_{5.4}F_{1.2}$, indicating that Rh exhibited better electron-capturing ability than Pd on the $Pb_2Ti_2O_{5.4}F_{1.2}$. More importantly, $Rh–Pd/Pb_2Ti_2O_{5.4}F_{1.2}$ exhibited much smaller Δabsorbance than $Rh/Pb_2Ti_2O_{5.4}F_{1.2}$, indicating that the electron-capturing property of Rh could be improved by Pd coloading and explaining the enhanced photocatalytic activity for H_2 evolution.

However, it is noted that the difference in H_2 evolution activity between the $Rh/Pb_2Ti_2O_{5.4}F_{1.2}$ and $Pd/Pb_2Ti_2O_{5.4}F_{1.2}$ under high light intensity conditions cannot simply be explained in terms of the electron-capturing ability of metal cocatalyst. The behavior of the $Pd/Pb_2Ti_2O_{5.4}F_{1.2}$ is somewhat strange, in that it showed relatively large fluctuation in the H_2 yield compared to the $Rh/Pb_2Ti_2O_{5.4}F_{1.2}$ and $Rh–Pd/Pb_2Ti_2O_{5.4}F_{1.2}$ under high light intensity conditions (Figure 2). This suggests that there are factors that are currently beyond our control regarding the preparation of $Pd/Pb_2Ti_2O_{5.4}F_{1.2}$ and its photocatalytic properties. At present, we could not fully elucidate photocatalytic behavior of the $Pd/Pb_2Ti_2O_{5.4}F_{1.2}$, which requires more systematic investigations such as the light intensity effect (although beyond the scope of the present work).

Figure 5. Current-voltage curves obtained from modified $Pb_2Ti_2O_{5.4}F_{1.2}$ electrodes under intermittent visible light ($\lambda > 400$ nm) in acetonitrile containing dissolved Et_4NBF_4, TEOA, and H_2O. Scan rate: 10 mV s^{-1}. Light source: 300 W Xe lamp. Irradiation area: 5.3 cm^2. [Ag/AgNO$_3$ at pH 7] = [NHE at pH 7] − 0.56.

Figure 6. Transient absorption intensity decay curves at 2000 cm^{-1} for modified $Pb_2Ti_2O_{5.4}F_{1.2}$ samples.

Conclusion

The $Pb_2Ti_2O_{5.4}F_{1.2}$ photocatalyst exhibited improved visible-light-induced H_2 evolution activity when loaded with various metal cocatalysts. Among the examined cocatalysts, Rh exhibited the best performance, and coloading with Pd further improved the activity. Photoelectrochemical and transient absorption spectroscopy measurements revealed that these cocatalysts effectively accelerate the photoreduction processes. In particular, the coloading of Pd improved the electron-capturing ability of Rh.

However, apparent quantum yield of the $Rh–Pd/Pb_2Ti_2O_{5.4}F_{1.2}$ photocatalyst was at most 0.25% at 420 nm even after optimization of the loading amount of Rh and Pd (see Figure S3 for the detail). Therefore, further development of the method for cocatalyst loading as well as for synthesis of $Pb_2Ti_2O_{5.4}F_{1.2}$ photocatalyst is required. It is also noted that at present, how the H_2 evolution occurs on the Rh–Pd cocatalyst remains unknown. A theoretical approach[25] may elucidate the reaction mechanism.

Experimental Section

Materials and reagents: PbO (99.9%) and TiO_2 (rutile, 99.99%) were purchased from Rare Metallic. PbF_2 (99.9%) was purchased from Mitsuwa Pure Chemicals. NaCl (>99.5%), acetonitrile (MeCN; >99.5%), and TEOA (>98.0%) were purchased from Kanto Chemical Co. CsCl (>99.9%) was purchased from Wako Pure Chemicals. For the loading of metal cocatalysts, $Ni(NO_3)_2\cdot6H_2O$ (>99.5%, Kanto Chemical), $RuCl_3\cdot3H_2O$ (>36% as Ru, Wako Pure Chemical Industries), $Na_3RhCl_6\cdot nH_2O$ (17.4% as Rh, Mitsuwa Pure Chemicals), $Na_2PdCl_4\cdot3H_2O$ (>95.0%, Wako Pure Chemical Industries), $Na_2IrCl_6\cdot6H_2O$ (>34.0% as Ir, Wako Pure Chemical Industries), $H_2PtCl_6\cdot6H_2O$ (98.5%, Kanto Chemical), and $HAuCl_4\cdot4H_2O$ (99%,

Chemistry–A European Journal

Research Article
doi.org/10.1002/chem.202200875

Chemistry Europe
European Chemical
Societies Publishing

Kanto Chemical) were used. All chemicals were used without further purification.

Synthesis of Pb$_2$Ti$_2$O$_{5.4}$F$_{1.2}$ and alkaline chloride treatment: The Pb$_2$Ti$_2$O$_{5.4}$F$_{1.2}$ photocatalyst was synthesized by a solid-state method.[26] PbO, TiO$_2$, and PbF$_2$ were mixed in a molar ratio of 1.4:2:0.6 and ground under methanol. The mixture was pelletized and then heated in an evacuated Pyrex tube with Pt foil at 823 K for 12 h (ramp rate of 10 K min^{-1}).

The as-synthesized Pb$_2$Ti$_2$O$_{5.4}$F$_{1.2}$ (250 mg), NaCl, and CsCl were mixed in a Pb$_2$Ti$_2$O$_{5.4}$F$_{1.2}$:NaCl:CsCl molar ratio of 1:1.4:2.6 and then ground. The mixture was subsequently sealed in an evacuated Pyrex tube, which was heated at 723 K for 5 h (ramp rate of 1 K min^{-1}). After the mixture naturally cooled to room temperature, the product was separated from the residual alkaline chloride by washing with distilled water several times, and was finally dried in an oven at 343 K. This NaCl-CsCl treatment has been reported to improve the photocatalytic activity of Pb$_2$Ti$_2$O$_{5.4}$F$_{1.2}$ for H$_2$ evolution, because of alkaline titanate species formed by the treatment on the Pb$_2$Ti$_2$O$_{5.4}$F$_{1.2}$ that offer favorable reaction sites for proton reduction.[16] In the present work, the NaCl-CsCl-treated Pb$_2$Ti$_2$O$_{5.4}$F$_{1.2}$ was used as a photocatalyst.

Characterization: A scanning electron microscope (SU9000 (Hitachi)) equipped with an EDS apparatus (EDAX, TEAM™ EDS system) was used to investigate the morphology and elemental distribution of the materials. XPS was conducted using an ESCA-3400 X-ray photoelectron spectrometer (Shimadzu). The binding energies were calibrated by referencing the C 1s peak (285.0 eV) for each sample.

Rh and Pd K-edge XAFS measurements were conducted on the BL-14B2 beamline of SPring-8 (Proposal No. 2020A1895). The X-ray absorption spectra were recorded in fluorescence mode at room temperature using a Si(311) two-crystal monochromator. A pair of Rh-coated mirrors were used to eliminate higher harmonics. The XANES spectra were analyzed using the Athena software package.[27]

Transient absorption measurements were conducted using a purpose-built spectrometer described previously.[23] The experimental details are given elsewhere.[28] Briefly, photocatalyst samples coated onto a CaF$_2$ plate at a density of 1.5 mg cm^{-2} were photoexcited under N$_2$ (20 Torr) using 420 nm pulses from a Nd: YAG laser (Continuum Surelite; duration, 6 ns; power, 5 mJ; repetition rate, 1 Hz).

Photocatalytic reactions: Photocatalytic reactions were conducted in a merry-go-round-type reaction apparatus using an LED (365 nm) light source, Iris-MG (CELL System), for the purpose of first screening metal cocatalysts. Metal cocatalysts were loaded on the surface of Pb$_2$Ti$_2$O$_{5.4}$F$_{1.2}$ by an in situ photodeposition method.[29] In each trial, 4 mg of Pb$_2$Ti$_2$O$_{5.4}$F$_{1.2}$ was dispersed in a test-tube reaction cell (11 mL capacity) containing 4 mL of reaction solution (MeCN:TEOA:H$_2$O=89:10:1, v/v/v). The use of MeCN as the main solvent is to ensure good dispersion of the hydrophobic Pb$_2$Ti$_2$O$_{5.4}$F$_{1.2}$ particles.[4] The precursor of the metal was dissolved in the reaction solution at a ratio of 0.5 wt% with respect to the Pb$_2$Ti$_2$O$_{5.4}$F$_{1.2}$ unless otherwise stated. After the solution was purged with Ar gas, it was irradiated with LED light for 20 h. The generated gases were analyzed using a gas chromatograph equipped with a thermal conductivity detector (GL Science GC323).

Photocatalytic reactions were also conducted using a Pyrex top-irradiation reaction vessel connected to a closed gas circulation system. In each trial, 100 mg of the photocatalyst was suspended in 140 mL of MeCN-TEOA mixed solution (13:1 v/v) containing 1 mL of water and a precursor of a metal source. After the solution was outgassed, it was irradiated with UV light ($\lambda > 350$ nm) for 10 h

using a 300 W Xe lamp (Cermax, PE300BF) fitted with a cold mirror (CM-1), where an output current of 20 A was applied. After the 10 h UV irradiation and subsequent removal of gaseous products, the photocatalyst suspension was irradiated with visible light ($\lambda > 400$ nm) passed through a cutoff filter (L42). The evolved gases were analyzed by gas chromatography (GC-8 A equipped with a thermal conductivity detector and an MS-5 A column (Shimadzu)); Ar was used as the carrier gas. Apparent quantum yield was measured in the same manner as reported previously.[16]

Photoelectrochemical measurements: Photoelectrochemical measurements were carried out with a potentiostat (HZ-pro, Hokuto Denko) and an electrochemical cell at room temperature. The cell was made of Pyrex glass and was a three-electrode-type system with a Pt wire and a Ag/AgNO$_3$ electrode as the counter and reference electrodes, respectively. The working electrode, Pb$_2$Ti$_2$O$_{5.4}$F$_{1.2}$/FTO, was prepared by an electrophoretic deposition method according to our previous method,[16] with some modifications (time of deposition, 2.5 min; without TiCl$_4$ treatment). A mixed solution of MeCN-TEOA-H$_2$O (130:10:1 v/v/v) dissolved with 0.1 M tetraethylammonium tetrafluoroborate (Et$_4$NBF$_4$; 99%, Sigma-Aldrich) was used as the electrolyte solution and was saturated with Ar gas prior to the electrochemical measurements. The light source was a 300 W Xe lamp (Cermax, PE300BF) equipped with a cutoff filter (L42) to emit visible light. The irradiation area was ~5.3 cm^2.

Acknowledgements

Conflict of Interest

The authors declare no conflict of interest.

Data Availability Statement

The data that support the findings of this study are available from the corresponding author upon reasonable request.

[1] J. Cui, C. Li, F. Zhang, *ChemSusChem* **2019**, *12*, 1872–1888.
[2] H. Kageyama, K. Hayashi, K. Maeda, J. P. Attfield, Z. Hiroi, J. M. Rondinelli, K. R. Poeppelmeier, *Nat. Commun.* **2018**, *9*, 772.
[3] A. Miyoshi, K. Maeda, *Solar RRL* **2021**, *5*, 2000521.
[4] R. Kuriki, T. Ichibha, K. Hongo, D. Lu, R. Maezono, H. Kageyama, O. Ishitani, K. Oka, K. Maeda, *J. Am. Chem. Soc.* **2018**, *140*, 6648–6655.
[5] H. Wakayama, K. Utimula, T. Ichibha, R. Kuriki, K. Hongo, R. Maezono, K. Oka, K. Maeda, *J. Phys. Chem. C* **2018**, *122*, 26506–26511.
[6] M. Hara, J. Nunoshige, T. Takata, J. N. Kondo, K. Domen, *Chem. Commun.* **2003**, 3000.
[7] K. Maeda, K. Teramura, D. Lu, T. Takata, N. Saito, Y. Inoue, K. Domen, *Nature* **2006**, *440*, 295.

[8] X. Zong, H. Yan, G. Wu, G. Ma, F. Wen, L. Wang, C. Li, *J. Am. Chem. Soc.* **2008**, *130*, 7176–7177.

[9] K. Maeda, X. Wang, Y. Nishihara, D. Lu, M. Antonietti, K. Domen, *J. Phys. Chem. C* **2009**, *113*, 4940–4947.

[10] K. Maeda, M. Higashi, D. Lu, R. Abe, K. Domen, *J. Am. Chem. Soc.* **2010**, *132*, 5858–5868.

[11] S. Yin, J. Han, Y. Zou, T. Zhou, R. Xu, *Nanoscale* **2016**, *8*, 14438–14447.

[12] K. Maeda, *J. Photochem. Photobiol. C* **2011**, *12*, 237–268.

[13] J. Yang, D. Wang, H. Han, C. Li, *Acc. Chem. Res.* **2013**, *46*, 1900–1909.

[14] K. Maeda, K. Teramura, D. Lu, N. Saito, Y. Inoue, K. Domen, *Angew. Chem. Int. Ed.* **2006**, *45*, 7806–7809; *Angew. Chem.* **2006**, *118*, 7970–7973.

[15] S. Teratani, J. Nakamichi, K. Taya, K. Tanaka, *Bull. Chem. Soc. Jpn.* **1982**, *55*, 1688–1690.

[16] H. Wakayama, K. Kato, K. Kashihara, T. Uchiyama, A. Miyoshi, H. Nakata, D. Lu, K. Oka, A. Yamakata, Y. Uchimoto, K. Maeda, *J. Mater. Chem. A* **2020**, *8*, 9099–9108.

[17] N. Hirayama, H. Nakata, H. Wakayama, S. Nishioka, T. Kanazawa, R. Kamata, Y. Ebato, K. Kato, H. Kumagai, A. Yamakata, K. Oka, K. Maeda, *J. Am. Chem. Soc.* **2019**, *141*, 17158–17165.

[18] J. R. Renzas, W. Huang, Y. Zhang, M. E. Grass, D. T. Hoang, S. Alayoglu, D. R. Butcher, F. F. Tao, Z. Liu, G. A. Somorjai, *Phys. Chem. Chem. Phys.* **2011**, *13*, 2556–2562.

[19] Y. Qi, J. Wu, H. Zhang, Y. Jiang, C. Jin, M. Fu, H. Yang, D. Yang, *Nanoscale* **2014**, *6*, 7012–7018.

[20] Y. Xu, T. Ge, H. Ma, X. Ding, X. Zhang, Q. Liu, *Electrochim. Acta* **2018**, *270*, 110–119.

[21] R. Nakamura, T. Tanaka, Y. Nakato, *J. Phys. Chem. B* **2005**, *109*, 8920–8927.

[22] K. Maeda, H. Hashiguchi, H. Masuda, R. Abe, K. Domen, *J. Phys. Chem. C* **2008**, *112*, 3447–3452.

[23] A. Yamakata, T.-a. Ishibashi, H. Onishi, *J. Phys. Chem. B* **2001**, *105*, 7258–7262.

[24] K. Furuhashi, Q. Jia, A. Kudo, H. Onishi, *J. Phys. Chem. C* **2013**, *117*, 19101–19106.

[25] D. Wang, Z.-P. Liu, W.-M. Yang, *ACS Catal.* **2018**, *8*, 7270–7278.

[26] K. Oka, H. Hojo, M. Azuma, K. Oh-ishi, *Chem. Mater.* **2016**, *28*, 5554–5559.

[27] B. Ravel, M. Newville, *J. Synchrotron Radiat.* **2005**, *12*, 537–541.

[28] Y. Tang, K. Kato, T. Oshima, H. Mogi, A. Miyoshi, K. Fujii, K. I. Yanagisawa, K. Kimoto, A. Yamakata, M. Yashima, K. Maeda, *Inorg. Chem.* **2020**, *59*, 11122–11128.

[29] B. Kraeutler, A. J. Bard, *J. Am. Chem. Soc.* **1978**, *100*, 4317–4318.